Royal Norwegian Council
for Scientific and Industrial Research
(NTNF)

NORSAR

NORSAR Scientific Report No. 2-87/88

Semiannual Technical Summary

1 October 1987 – 31 March 1988

L.B. Loughran (ed.)

Kjeller, June 1988

VII. SUMMARY OF TECHNICAL REPORTS / PAPERS PUBLISHED

VII.1 On exploitation of small-aperture NORESS type arrays for enhanced P-wave detectability

Introduction

Under potential future nuclear test bans, small-aperture NORESS type arrays can provide significant contribution to the performance of the monitoring system. By their ability to detect, locate and characterize weak seismic signals, the probability of a successful treaty evasion can be considerably reduced.

In this paper, we concentrate on the detection aspect of small-aperture (regional) arrays, and focus on detection of primary phases preceded by pure noise. By beamforming, we can exploit the incoherent structure of seismic noise and the coherent structure of P-arrivals to enhance the signal-to-noise ratio (SNR). On the other hand, detection of secondary phases from events at regional distances (up to 2000 km) will not be addressed in this paper, since they in most cases are not embedded in pure noise, but in the relatively coherent coda of the preceding signal arrivals. SNR enhancement by beamforming will not be efficient for these phases unless the single station noise level is higher than the coda level. Under such conditions, the noise can be efficiently suppressed until the level of the underlying coda is reached.

To realistically assess the potential of the NORESS array for event detection, it is necessary to compute the actual beamforming gains for a variety of representative seismic signals. From such calculations, the objective is to infer the best set of beams for the detection of regional and teleseismic P-waves. The results from this study can then be applied to other arrays of the NORESS type.

NORESS design considerations -- a brief review

The design of the NORESS array involved balancing of several partly conflicting demands on array performance. For details, see Followill and Harris (1983), and Mykkeltveit (1985).

Under the condition of equal signal and noise amplitudes at each sensor, we can express the beamforming gain G by the normalized zero-lag cross-correlations via the formula:

$$G^2 = \sum_{i,j=1}^{N} C_{ij} \Big/ \sum_{i,j=1}^{N} \rho_{ij}$$

where C_{ij} is the signal correlation between sensors i and j, and ρ_{ij} is the corresponding noise correlation. Numerical models for these correlations as a function of intersensor separation were constructed for several filter bands based on data from a provisional installation at NORSAR subarray 06C, see Mykkeltveit et al (1983). Some important findings from these investigations were that the noise correlation curves consistently had negative minima at certain interstation separations before tending to zero at larger separation distances, while the signal correlations degraded continuously as the distances increased, see Fig. VII.1.1. These results indicated a possibility for noise suppression in excess of $\sqrt{N}$ which is the theoretically expected value if all noise cross-correlations were 0. If the signal decorrelation was sufficiently small, SNR gains also in excess of $\sqrt{N}$ could be obtained.

In addition to the constraint that the array should have an equal capability to process signals from all directions (symmetry), it was required that the SNR enhancement (gain) by beamforming should be close to optimum for a wide range of frequencies (1-10 Hz). It was then realized that the array should consist of instruments where a large span of intersensor separations were represented, and that sub-

configurations of the array must be used to detect different phases in different frequency bands. This study deals with how one should exploit the sub-configurations to achieve the best SNR gain for P-phases in different frequency bands, and to quantify the gain values.

The array's ability to estimate the apparent velocity and azimuth of seismic signals, to resist spatial aliasing, to properly sample the wavefield and to have an option for a good three-component subarray were also considered important factors in the design work. From the criteria outlined above, it was decided to build an array with a geometry based on four concentric rings spaced at log-periodic intervals in radius R, according to the relation:

$$R = R_{min} \cdot \alpha^n, \; n = 0,1,2,3, \quad R_{min} = 150 \text{ m}, \quad \alpha = 2.15$$

The final configuration of the NORESS array, shown in Fig. VII.1.2, has 3 elements in the innermost ring called the A-ring (radius 150 m), 5 elements in the B-ring (radius 320 m), 7 in the C-ring (radius 690 m), 9 in the D-ring (radius 1490 m), plus one in the center, called A0. A0, C2, C4 and C7 are all equipped with three-component instrumentation.

Data analysis procedure

Applying a short-term to long-term average (STA/LTA) algorithm to a set of filtered beams has proved to be a robust and reliable way of detecting seismic signals. In this study we want to link the calculation of SNR gain, noise suppression and signal loss by beamforming to the current operational detection algorithm, and hence avoid indirect measurement methods. The analysis procedure has been as follows:

1. Twelve partly overlapping filter bands that in our general experience have appeared most appropriate for regional and teleseismic P-wave detection were defined, see Table VII.1.1.

Three years of routine processing of regional array data from NORESS have shown that P-waves can have dominant frequencies varying from below 1.0 Hz to well above 10 Hz. This observation together with results from a previous study by Kværna and Mykkeltveit (1986), formed the basis for the selection of the filter bands.

2. From the 25 short-period vertical component instruments of the NORESS array, ten sub-geometries that appeared reasonable in the detection process were used to form beams in the respective twelve filter bands. These sub-geometries were symmetric, so all elements of each array ring had either weight 1 or weight 0, see Table VII.1.2.

3. For each of the twelve frequency bands, five high SNR regional and/or teleseismic P-wave signals were selected, see Table VII.1.3. The events were all found by searching through the bulletins generated from real-time processing of NORESS data. Events with peak signal frequencies close to the lower cutoff of the bands were chosen. This was done in order to ensure that the signal was analyzed in the band for which the SNR for that signal attains its maximum value. The approach chosen satisfied this requirement, since the noise amplitudes almost always decrease monotonically with increasing frequencies in the range of interest for this study.

   In the search for representative events for each filter band, it turned out, as expected, that teleseismic events fully dominated the frequency range up to 2 Hz. In the range between 2 and 5 Hz, both teleseismic and regional events were present, whereas teleseismic events were almost absent for frequencies above 5 Hz.

4. The beamforming steering delays for all events were calculated using the wide-band slowness estimation method (Kværna and

Doornbos, 1986). The apparent velocity and azimuth of each P-phase was estimated by processing all 25 channels in the frequency band representative for that event, see 3) above.

5. All events were then subjected to STA/LTA detection processing using a new program system developed at NORSAR (Fyen, 1987). The SNR, STA and LTA detection values for all beams as well as for all single channels were stored to compute the SNR gain, noise suppression and signal loss. The SNR (STA/LTA) gain was defined as the SNR of the beam divided by the average SNR of the single channels applied in the beamforming. The corresponding noise suppression was defined as the average LTA of the single channels applied in the beamforming divided by the LTA of the beam, while the signal loss was defined as the similar ratio of STA values. When expressing the values in decibels, the following relation holds:

SNR gain = Noise suppression - Signal loss

Table VII.1.4 shows the output from processing one of the sixty events in the data base.

Detailed presentation of results for two geometries

When plotting the noise suppression values for all events as a function of the lower cutoff of the filter band applied in the analysis, we get for the full array configuration (A0Z, A-ring, B-ring, C-ring and D-ring) the representation shown in Fig. VII.1.3a. As seen from the spread of the five values of each filter band, some averaging must be done to produce meaningful results. Some of the filters show differences up to 5 dB. After calculating the mean of the values within each of the twelve passbands and introducing some slight smoothing, the curve in Fig. VII.1.3a was obtained. Rather than progressing with the

discrete measurement points, we will mostly present and apply the smoothed curves in the following presentation and discussion.

In the full array configuration, a large span of intersensor separations are represented. As seen from Fig. VII.1.3a, the $\sqrt{N}$ noise suppression level was not reached for frequencies below 3.5 Hz. This is due to the fact that at such frequencies, the noise is correlated between some of the sensors, and even though some of the sensor pairs produce negative correlations, the total noise suppression does not reach the $\sqrt{N}$ level (13.98 dB for 25 sensors).

The noise suppression for the sub-geometry A0Z, C-ring and D-ring is given in Fig. VII.1.3b. In contrast to the results using the full array, we here achieved values in excess of $\sqrt{N}$ (now 12.3 dB for 17 sensors) in the frequency band 1 to 4 Hz. For this sub-geometry, only relatively large intersensor separations (700 m or more) are represented, which in the band 1 to 4 Hz have negative noise cross-correlations. Negative cross-correlations imply destructive interference when forming a beam. Above 4 Hz the noise suppression curve approaches the $\sqrt{N}$ level, which is consistent with an assumption of uncorrelated noise.

Figs. VII.1.3c and VII.1.3d give the signal loss for the two configurations discussed above. The signal losses are less than 1 dB for frequencies up to about 3 Hz, at which point the signal decorrelation starts to increase for both configurations.

Finally, the SNR gain curves are given in Figs. VII.1.3e and VII.1.3f. The full array does not reach the $\sqrt{N}$ level for any frequency. When the noise suppression finally reaches this level at about 3.5 Hz, the signal loss is exceeding 1.5 dB. For the sub-geometry A0Z, C-ring and D-ring the signal loss is negligible between 1 and 3 Hz. In this frequency band, the noise suppression is exceeding $\sqrt{N}$, and the SNR-gain is therefore also exceeding this value.

Composite gain curves

In determining which sub-geometry should be utilized to achieve optimal beamforming gain in the different frequency bands, it is necessary to directly compare the absolute gain values. The question of beamforming gain relative to $\sqrt{N}$ serves more as an indicator of the noise field characteristics, and is therefore more relevant in the array design phase. Now, it turns out that in order to cover the entire 0-10 Hz band, only four different sub-geometries (out of the ten considered) are needed, and each of which provides the highest absolute SNR gain within a certain frequency interval. This result is presented in Fig. VII.1.4 in the form of a composite gain curve, along with the corresponding composite curves for the noise suppression and signal loss. The following comments apply regarding the four frequency intervals given in Fig. VII.1.4.

0.5-1.0 Hz: To guard against the relatively high noise spectral level in the lower part of this band, the NORESS system response is designed with a strong rolloff. Therefore the dominant recorded noise amplitudes seldom have frequencies below 0.8 Hz, so a filter band, e.g., from 0.8 to 1.6 Hz would probably produce similar results. Nevertheless, for frequency bands with lower cutoffs below 1.0 Hz, the A0Z, D-ring configuration is capable of producing array gains between 9 and 12 dB. The signal loss is negligible in this frequency band.

1.0-2.3 Hz: For detection of the teleseismic signals that are abundant in this frequency range, beamforming applying the A0Z, C-ring and D-ring geometry provides SNR enhancement of about 13 dB. Under favorable noise conditions, almost 15 dB has been measured. The signal loss is less than 1 dB, and the noise suppression is well above the $\sqrt{N}$ level of 12.3 dB (17 sensors).

2.3-5.0 Hz: Intersensor separations introduced by adding the B-ring enhance the noise suppression for frequencies above 2.3 Hz, so the SNR gain is still kept at about 13 dB out to about 3.5 Hz. Between 3.5 and 4.0 Hz, the signal loss increases sharply to more than 2 dB, and the best SNR gain curve produced by the A0Z, B-ring, C-ring and D-ring sub-geometry drops to about 11 dB at 5 Hz.

5.0-10.0 Hz: The full array noise suppression stays at the $\sqrt{N}$ level (13.98 dB) in almost the entire band. Even though the signal decorrelation starts to be significant for frequencies above 6 Hz, the full array provides the best SNR gain all the way out to 10 Hz. The gain values stay at about 11 dB from 5 to 7 Hz, and then drop to 8.5 dB at 10 Hz.

Comparison of different array geometries

The main emphasis of this study has been on determining optimum sub-geometries in various frequency bands and corresponding SNR gains for a full NORESS-type array. However, the study has in addition provided a basis for comparing the projected performance of regional arrays of different sizes. Thus, we have compared optimum SNR gains for the following three arrays:

i) A full regional array (NORESS type)
   Diameter: 2980 m
   Number of instruments: 25
   Geometry: A0Z, A-ring, B-ring, C-ring, D-ring

ii) An intermediate regional array
   Diameter: 1390 m
   Number of instruments: 16
   Geometry: A0Z, A-ring, B-ring, C-ring

iii) A small regional array

Diameter: 650 m

Number of instruments: 9

Geometry: A0Z, A-ring, B-ring

SNR gains by the full array have already been discussed. For the intermediate and small arrays, processing to determine optimum SNR gains was done as for the full array, but taking into account only those instruments included in the respective array configurations.

First we consider the intermediate array, i.e., all subgeometries with the D-ring excluded. The results given in Fig. VII.1.5a are consistent with the findings when processing the full array, see Fig. VII.1.4. Out to 2.3 Hz, the A0Z and C-ring is the best sub-geometry, then the B-ring instruments start to contribute positively and gain values between 10 and 12 dB are achieved to about 5 Hz. In the frequency band 5 to 10 Hz, all available rings (A0Z, A-ring, B-ring and C-ring) should be included.

In analyzing the performance of the small array, we excluded both the C-ring and the D-ring in the selection of sub-geometries. From Fig. VII.1.5b, it turns out that 6.5 to 8 dB SNR gain is produced between 3.5 and 10 Hz. The best sub-geometry below 5 Hz comprises A0Z and the B-ring, whereas the A-ring starts to contribute positively above 5 Hz. Again, this frequency dependency of the optimum sub-geometry is consistent with the overall trend noticed for the full and intermediate arrays.

Conclusions

This study has demonstrated that the NORESS array geometry provides P-phase signal-to-noise ratio (SNR) gains (relative to the average single sensor) of 10 dB or more over almost the entire frequency range 0.5-

10 Hz, the only exception being slightly lower gains at the low and high end of this band.

In the frequency range 1-4 Hz, which is by far the most important both for regional and teleseismic P-phase detection, these gains are consistently as high as 12-14 dB, i.e., 0.6-0.7 m_b units. Such an excellent performance over a wide range of frequencies is to our knowledge unmatched by any previous array design.

As described in this paper, and illustrated in Fig. VII.1.4, these SNR gains are obtained through beamforming on selected subarrays, where the choice of subarray is governed exclusively by the frequency range considered.

As expected, some of the rings produce intersensor separations that should be avoided for certain frequency rantges. Below 1.0 Hz, all instruments except A0Z and the D-ring produce positive noise correlations and were therefore excluded. At 1 Hz, the C-ring starts to contribute to an increased SNR gain, at about 2.3 Hz, the B-ring and finally at 5 Hz, the A-ring.

The main reason why the subsets of the array, at lower frequencies, outperform the full array lies in the spatial noise correlation properties. As is well known, the beam SNR may actually deteriorate if too many highly correlated sensors are included in the beamforming process. The procedure outlined in this paper, where a number of different bandpass filters are applied in parallel, and the beams are based on the best sub-geometry for each frequency band, ensures excellent SNR gain and signal detection performance at all frequencies.

A comparison of the projected overall performance of the full NORSESS array and two smaller arrays (denoted the intermediate and small array, respectively) has been carried out. The results, as summarized in Fig. VII.1.6, are as follows:

The intermediate array provides SNR gains relative to the average single sensor that exceed 8 dB in the 1.5-10 Hz frequency range. Thus, such an array would be very capable for regional P-phase detection, although somewhat inferior to the full NORESS-type array. The degradation in performance would be quite significant at frequencies below 3 Hz.

The small array configuration has SNR gains exceeding 6 dB in the range 3-10 Hz, but the performance is considerably lower than the two larger configurations, except at the very high frequency end, where the difference is modest.

Under the assumption that the beam is steered towards the azimuth and apparent velocity of the incoming P-phase, we know from the results presented in this paper which sub-geometry provides the best beamforming gain in each of the 12 filter bands. We also know which sub-geometries are best when discarding the D-ring or both the C-ring and D-ring from the selection.

This latter point is important, not only for the possible design of smaller arrays, but also in view of practical considerations when deploying a beam set to be processed in real time. The essential point here is that a smaller array geometry provides broader beam lobes, and thus requires fewer beams to be deployed for complete coverage. If the computer load is a limiting factor, the fewer beams might be an important tradeoff factor against the lower achievable SNR gains.

To arrive at a recommended beam deployment for the respective filter bands, the optimum values have to be seen in conjunction with other factors like mis-steering of the beams, false alarm rate and computer load. In future work, the dependencies between these factors and their implications on a final beam deployment will be studied in detail.

T. Kværna

References

Followill, F. and D.B. Harris (1983): Comments on Small Aperture Array Designs. Informal Report, Lawrence Livermore National Laboratory.

Fyen, J. (1987): Improvements and Modifications. Semiannual Technical Summary, 1 October 1986 - 31 March 1987, NORSAR Sci. Rep. No. 2-86/87, Kjeller, Norway.

Kværna, T. and D.J. Doornbos (1986): An integrated approach to slowness analysis with arrays and three-component stations. Semiannual Technical Summary, 1 October 1985 - 31 March 1986, NORSAR Sci. Rep. No. 2-85/86, Kjeller, Norway.

Kværna, T. and S. Mykkeltveit (1986): Optimum beam deployment for NORESS P-wave detection. Semiannual Technical Summary, 1 April - 30 September 1986, NORSAR Sci. Rep. No. 1-86/87, Kjeller, Norway.

Mykkeltveit, S. (1985): A new regional array in Norway: Design work and results from analysis of data from a provisional installation. In: The VELA Program. A twenty-five year review of basic research. Ed. A.U. Kerr. Defense Advanced Research Projects Agency.

Mykkeltveit, S., K. Åstebøl, D.J. Doornbos and E.S. Husebye (1983): Seismic array configuration optimization. Bull. Seism. Soc. Am., 73, 173-186.

No.	Prototype	Type	Low	High	Order
BP01	BU	BP	0.5	1.0	3
BP02	BU	BP	1.0	2.0	3
BP03	BU	BP	1.5	3.0	3
BP04	BU	BP	2.0	4.0	3
BP05	BU	BP	2.5	5.0	3
BP06	BU	BP	3.0	6.0	3
BP07	BU	BP	3.5	7.0	3
BP08	BU	BP	4.0	8.0	3
BP09	BU	BP	5.0	10.0	3
BP10	BU	BP	6.0	12.0	3
BP11	BU	BP	8.0	16.0	3
BP12	BU	HP	10.0		3

Table VII.1.1 The table shows the twelve filters applied in the experiment; all were recursive Butterworth filters of order 3 with one octave bandwidth.

A0Z	A-RING	B-RING	C-RING	D-RING
1	0	0	0	1
1	0	0	1	1
1	0	1	1	1
1	1	1	1	1
1	0	0	1	0
1	0	1	1	0
1	1	1	1	0
1	0	1	0	0
1	1	1	0	0
1	1	0	0	0

Table VII.1.2 Array ring weights for the ten sub-geometries considered in this study.

ORIGIN DATE	ORIGIN TIME	LAT	LON	MAG	ARRIVAL TIME	APP VEL	AZIM	FILT	NO.
03/12/87	23.10.30.7	0.3S	18.1W	5.5	23.21.11.8	16.4	205.4	1	1
09/07/87	11.57.13.8	31.1S	178.1W	5.8	12.16.50.6	35.7	35.4	1	2
07/15/87	07.16.13.5	17.5N	97.1W	5.9	07.28.36.9	21.5	266.6	1	3
04/29/87	01.45.22.6	27.4N	56.1E	5.9	01.53.37.7	16.7	122.4	1	4
05/12/87	01.30.25.0	7.1N	126.7E	6.2	02.00.39.5	29.2	267.9	1	5
07/20/87	16.47.48.1	33.7N	57.0E	5.0	16.55.17.7	14.1	115.0	2	6
05/09/87	06.32.34.9	11.3S	165.7E	5.5	06.51.36.1	39.4	35.6	2	7
07/15/87	16.11.02.8	47.0N	154.1E	5.2	16.22.01.2	22.9	19.6	2	8
07/22/87	08.23.04.3	15.8N	93.4W	5.1	08.35.21.5	20.1	280.1	2	9
03/15/87	05.11.17.0	15.6N	94.6W	5.6	05.23.45.8	21.0	294.3	2	10
04/30/87	05.17.37.0	39.8N	74.6E	5.7	05.25.39.8	15.7	89.3	3	11
07/11/87	06.15.51.0	82.2N	17.6W	5.5	06.20.55.0	10.5	347.8	3	12
07/04/87	17.16.52.1	10.9N	62.2W	4.7	17.28.14.8	19.2	255.5	3	13
03/12/87	01.57.17.2	49.9N	78.8W	5.5	02.04.37.4	16.2	79.4	3	14
08/15/87	00.31.49.2	52.7N	152.6E	4.9	00.41.22.4	14.1	29.2	3	15
03/22/87	17.45.04.6	52.1N	171.4W	5.3	17.55.57.4	12.1	7.2	4	16
02/27/87	23.34.52.0	38.5N	20.3E	5.3	23.39.57.1	11.4	161.6	4	17
02/19/87	22.41.25.2	40.2N	21.6E	4.1	22.46.08.8	9.9	159.4	4	18
07/27/87	21.20.50.5	40.8N	22.1E	4.5	21.25.32.1	10.1	159.1	4	19
07/16/87	16.36.17.7	59.5N	28.0E	2.8	16.37.50.0	8.3	83.7	4	20
07/23/87	19.28.01.6	46.4N	153.5E	5.3	19.39.01.8	24.4	29.7	5	21
11/05/87	18.31.25.8	37.0N	21.4E	4.0	18.36.42.4	10.6	146.1	5	22
04/12/87	09.00.51.8	42.7N	26.6E	3.8	09.05.28.4	10.2	141.9	5	23
03/09/87	19.50.21.2	39.4N	20.5E	3.7	19.55.13.3	10.0	159.0	5	24
04/16/87	01.10.20.6	55.0N	158.0E	5.0	01.20.05.6	14.4	27.0	5	25
04/12/87	12.13.51.0	31.8N	75.8E	4.2	12.22.43.8	14.2	100.6	6	26
07/11/87	13.55.54.2	36.6N	26.8E	4.5	14.01.12.0	10.6	148.4	6	27
07/24/87	02.42.59.0	32.0N	75.5E	4.1	02.51.49.9	14.0	98.3	6	28
12/13/87	06.22.39.0	32.8N	73.9E	4.2	06.31.17.9	14.5	100.1	6	29
09/10/87	21.53.14.6	43.9N	147.8E	5.2	22.04.21.4	12.8	32.9	6	30
11/01/87	20.39.33.0	65.1N	11.9E	3.6	20.40.37.0	8.6	358.7	7	31
07/20/87	00.29.38.2	52.2N	156.3E	4.4	00.39.49.5	14.6	33.8	7	32
12/26/87	08.58.31.0	45.4N	152.5E	4.6	09.09.36.5	16.2	36.6	7	33
03/31/87	01.18.36.8	53.2N	156.5E	5.2	01.28.46.0	14.9	38.4	7	34
01/19/87	04.07.24.2	55.6N	5.6E	3.6	04.08.54.5	9.1	213.6	7	35

Table VII.1.3 (page 1 of 2) Events applied in the data analysis procedure. The analysis filter number (FILT) corresponds to the filters given in Table VII.1.1. The event locations were given by one of the following agencies: PDE, University of Helsinki, University of Bergen or NORESS automatic bulletin. In the cases where no location is given, the only availabe event information is a P-phase detected on the NORESS array.

09/04/87	08.38.18.8	61.4N	3.1E	3.4	08.39.20.8	9.4	289.6	8	36
04/24/87					11.59.42.9	9.1	130.3	8	37
03/01/87					12.49.39.0	16.7	107.0	8	38
07/16/87	12.07.54.5	60.1N	29.4E	2.6	12.10.01.6	9.0	76.6	8	39
07/06/87	22.48.49.4	60.0N	29.5E	2.6	22.50.58.4	11.2	83.3	8	40
07/03/87	10.38.49.6	59.5N	24.0E	3.0	10.40.23.3	9.7	106.7	9	41
07/25/87	19.08.32.1	60.1N	4.8E	2.1	19.09.24.4	9.4	253.3	9	42
04/18/87	02.51.08.6	61.6N	2.6E	2.4	02.52.12.4	9.5	292.9	9	43
07/22/87	21.36.35.4	61.0N	2.6E	2.6	21.37.38.6	9.4	285.1	9	44
04/19/87	22.16.20.2	57.1N	7.8E	3.2	22.17.23.0	8.0	203.3	9	45
04/25/87					16.30.56.7	8.2	196.3	10	46
03/01/87	06.42.03.0	57.1N	7.1E	3.5	06.43.07.7	9.0	211.8	10	47
08/31/87	17.32.59.9	59.7N	10.6E	1.7	17.35.08.3	7.1	209.0	10	48
07/07/87	01.44.40.4	60.2N	29.7E	2.7	01.46.50.4	12.1	82.9	10	49
05/25/87					04.14.34.2	8.7	182.4	10	50
05/25/87	04.26.04.5	57.7N	11.5E	2.8	04.28.12.0	8.7	179.5	11	51
01/19/88	07.00.54.1	62.3N	4.0E	2.5	07.03.01.8	9.6	288.2	11	52
08/01/87	19.57.29.3	57.5N	5.8E	2.2	19.59.39.3	8.2	204.6	11	53
01/12/88					09.04.40.1	8.9	186.7	11	54
01/16/88					13.26.34.4	8.7	181.6	11	55
02/04/87	12.02.41.0	61.7N	5.0E	3.5	12.03.33.0	9.6	294.3	12	56
05/25/87	02.35.26.4	61.8N	5.3E	3.1	02.36.15.9	9.8	297.0	12	57
01/07/88	12.51.09.8	59.5N	11.0E	1.6	15.53.16.7	7.0	199.4	12	58
10/31/87	10.09.14.1	61.1N	4.5E	4.2	10.10.07.4	9.5	289.2	12	59
12/01/87	12.08.00.6	59.3N	10.4E	1.6	12.10.10.0	6.8	206.0	12	60

Table VII.1.3 (page 2 of 2)

SNR-gain(dB)	Noise-suppression(dB)	Signal-loss(dB)	LTA	A0	A	B	C	D
9.03	10.53	1.50	31.7	1	0	0	0	1
14.67	15.69	1.02	17.3	1	0	0	1	1
12.76	13.58	0.82	21.6	1	0	1	1	1
10.88	11.60	0.72	26.9	1	1	1	1	1
9.04	9.38	0.34	34.8	1	0	0	1	0
7.84	8.11	0.27	39.4	1	0	1	1	0
6.67	6.90	0.23	45.0	1	1	1	1	0
2.85	2.95	0.10	68.8	1	0	1	0	0
2.06	2.16	0.10	75.7	1	1	1	0	0
0.48	0.53	0.05	92.1	1	1	0	0	0

Table VII.1.4 The table gives the SNR-gain, noise suppression, signal loss, the detection LTA value and the corresponding array ring weights from processing event number 13 (see Table VII.1.3). This is a teleseismic event which has been analyzed in the filter band 1.5-3.0 Hz.

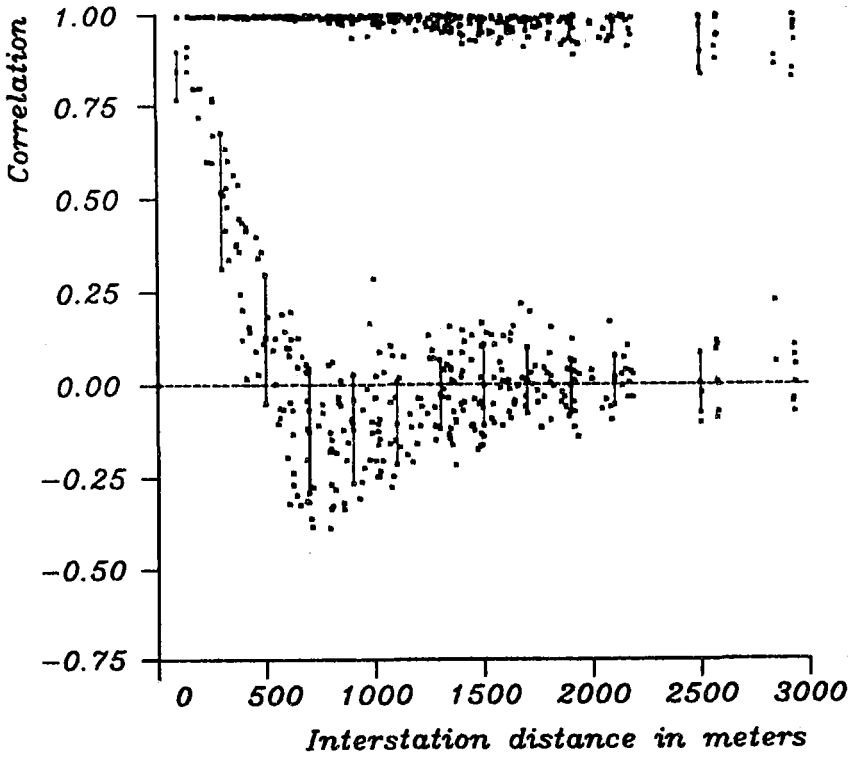

Fig. VII.1.1 Signal (upper part) and noise (lower part) correlations in the 2-4 Hz frequency band. The arrival time of the P-phase is 1985 - 115:01.02.27. After preshifting the traces with steering delays corresponding to the apparent velocity and azimuth of the incoming P-phase, the signal correlations were calculated from a 1 sec time window at the beginning of the P-phase. The noise correlations were calculated from a 60 sec long time window prior to the signal. The error bars reflect a scatter of plus/minus one standard deviation.

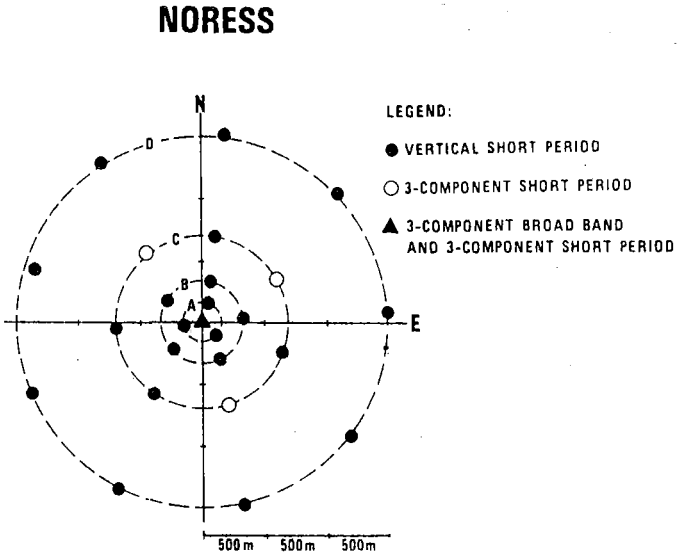

Fig. VII.1.2 The geometry of the NORESS array. The short period instrument at the center of the array is denoted A0. In this study, only the vertical short period instruments were applied.

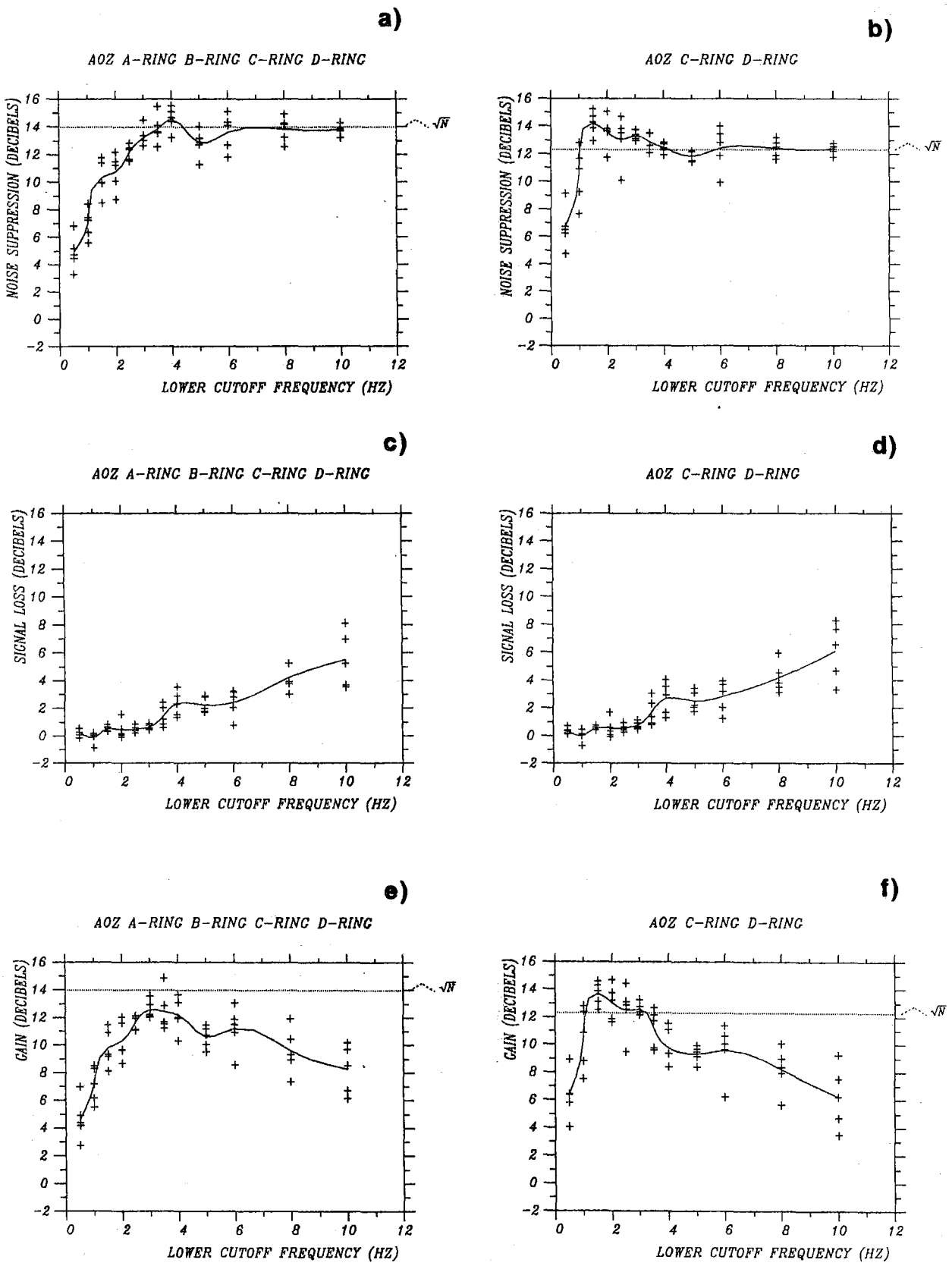

Fig. VII.1.3 Noise suppression, signal loss and SNR gain for the 25-element full array geometry (a,c,e) and for the 17-element AOZ, C-ring and D-ring sub-geometry (b,d,f).

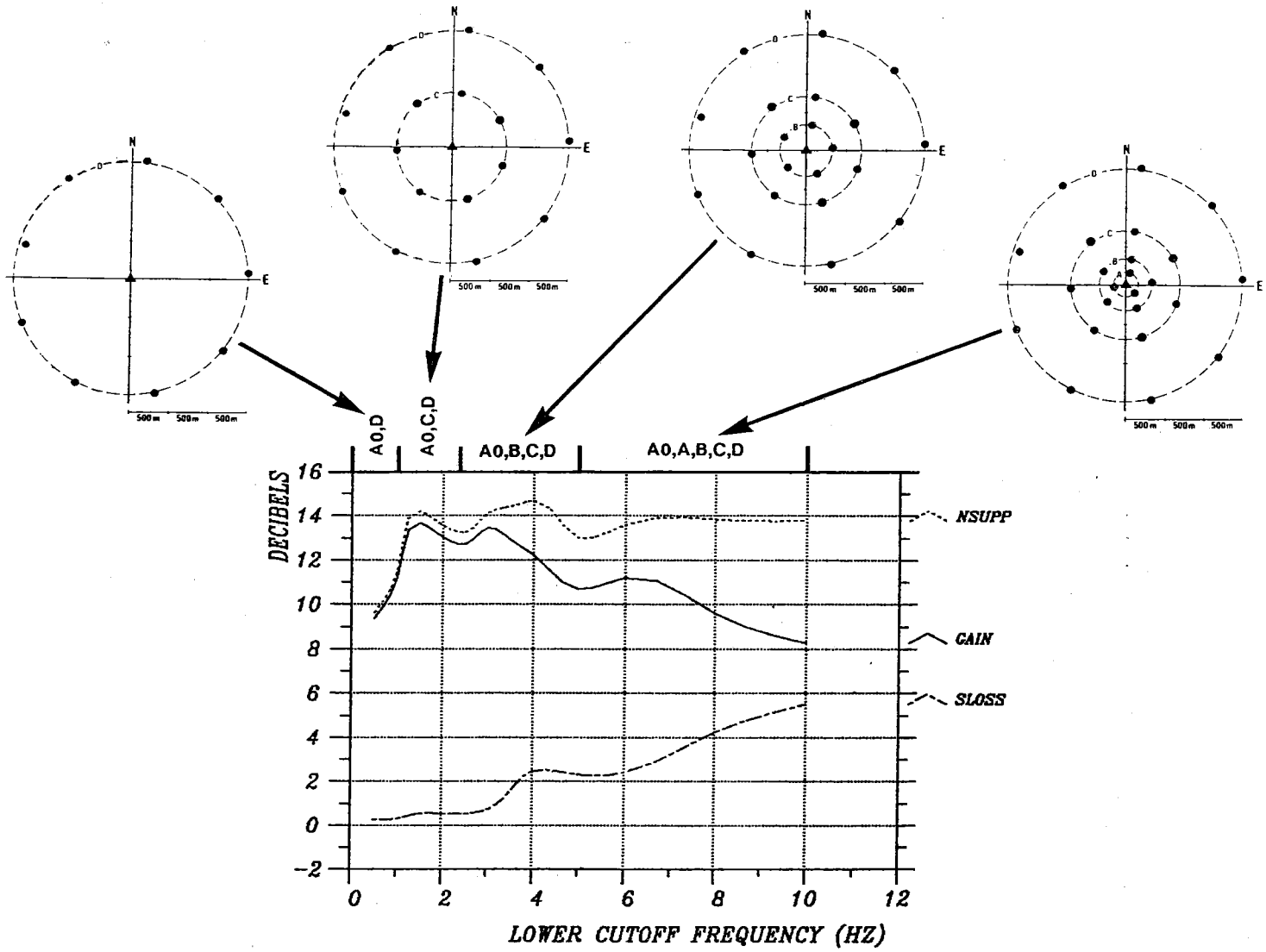

Fig. VII.1.4 The gain curve shown in this figure represents the best gain values produced by any of the ten sub-geometries. In addition, we have also given the corresponding noise suppresion (NSUPP) and signal loss (SLOSS). The best sub-geometries are shown above, and the arrows point to the frequency interval where they provide the highest SNR gain.

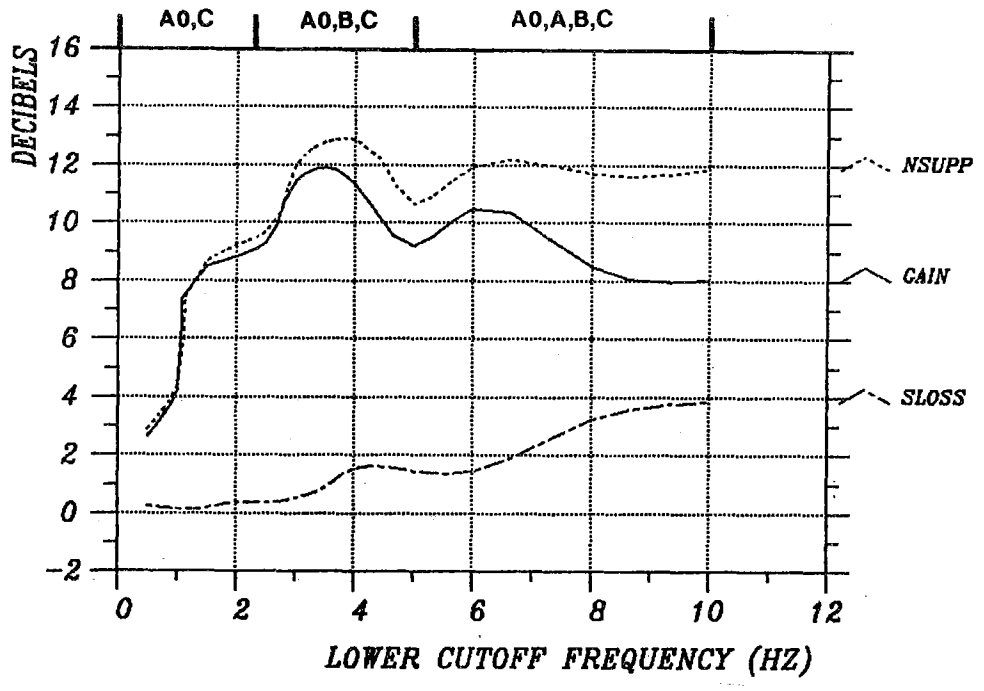

Fig. VII.1.5a The gain curve represents the best gain values when searching from sub-geometries with the D-ring excluded. In addition, the corresponding noise suppression (NSUPP) and signal loss (SLOSS) are given. The best sub-geometries and their frequency interval (A0Z,C denotes A0Z, C-ring) are given above.

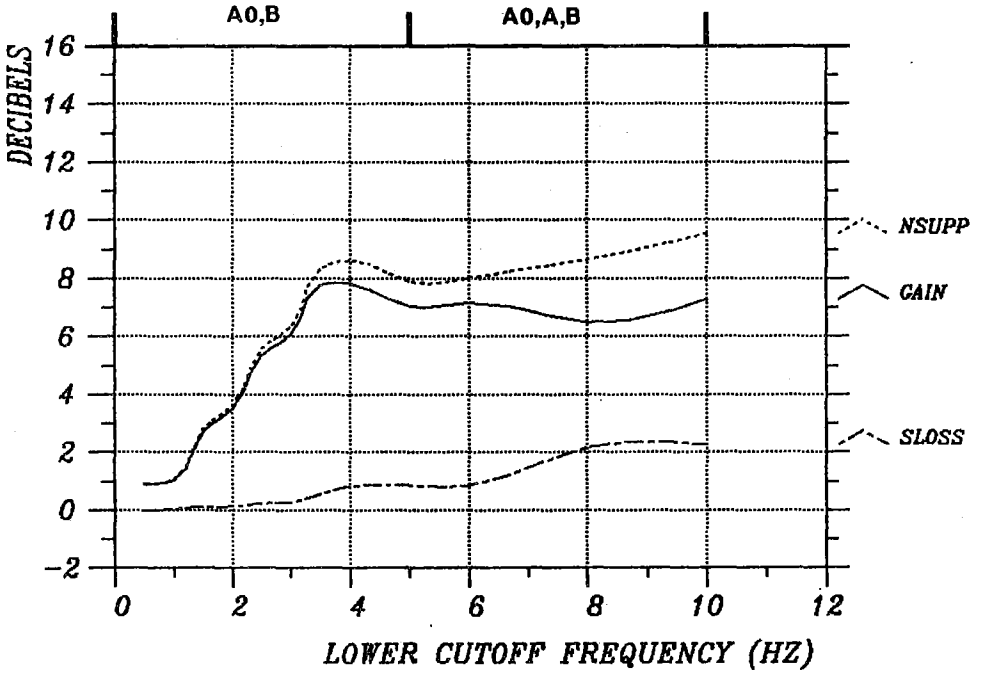

Fig. VII.1.5b Same as Fig. VII.1.5a, but now with both C-ring and D-ring excluded.

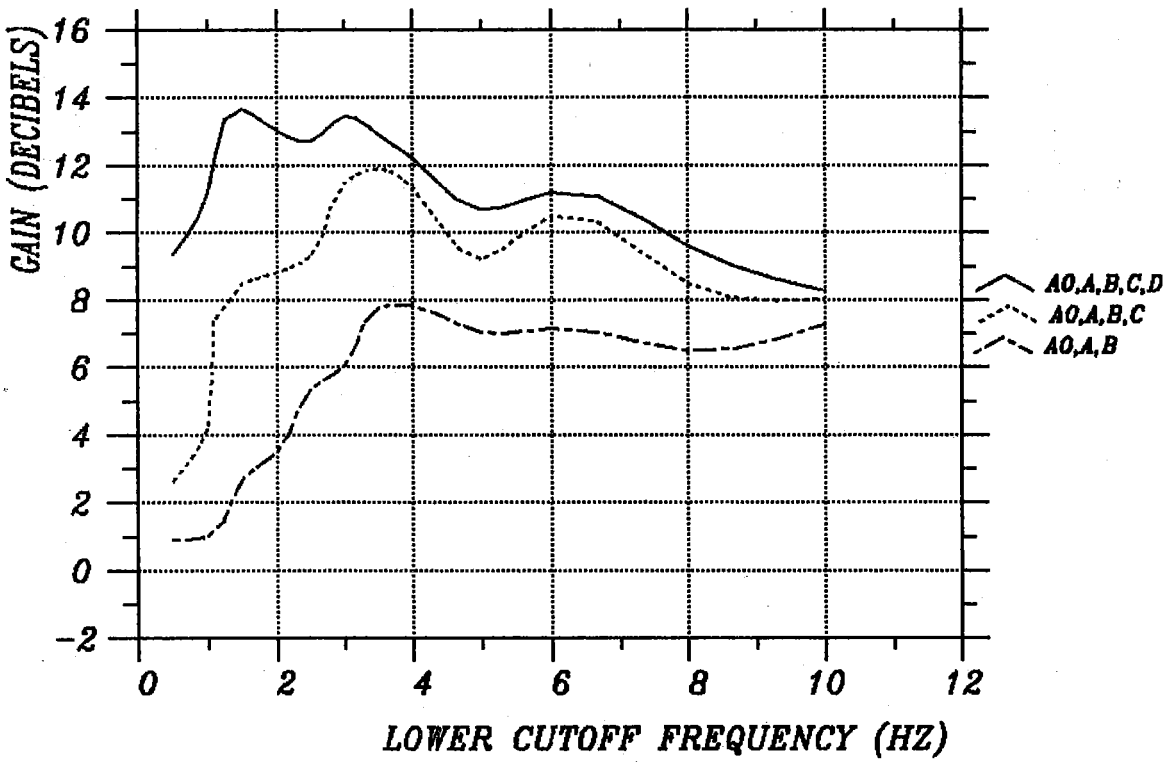

Fig. VII.1.6 The best gain curve based on the full NORESS geometry and also shown in Fig. VII.1.4, is given by the upper solid curve. The gain produced with the D-ring excluded is given by the dotted curve in the middle. We can see that up to about 3 Hz, the gain is well below the best, but for frequencies above 3 Hz, it stays only 1 to 2 dB below. The gain produced with both the C- and D-rings excluded is given by the lower closed dotted curve. As seen from the figure, it is more than 3 dB below the best for all frequencies up to 8 Hz, but between 8 and 10 Hz it comes closer to the best values.